

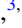






## Nanoscale magnetic bubbles in Nd<sub>2</sub>Fe<sub>14</sub>B at room temperature

Yangkun He <sup>1,\*</sup>, Toni Helm <sup>1,2</sup>, Ivan Soldatov <sup>3,4</sup>, Sebastian Schneider <sup>5,3</sup>, Darius Pohl <sup>5</sup>, Abhay Kant Srivastava,<sup>6</sup>  
Ankit Kumar Sharma <sup>6</sup>, Johannes Kroder,<sup>1</sup> Walter Schnelle,<sup>1</sup> Rudolf Schaefer,<sup>3,7</sup> Bernd Rellinghaus <sup>5</sup>,  
Gerhard H. Fecher,<sup>1</sup> Stuart S. P. Parkin,<sup>6</sup> and Claudia Felser<sup>1</sup>

<sup>1</sup>Max-Planck-Institute for Chemical Physics of Solids, 01187 Dresden, Germany

<sup>2</sup>Dresden High Magnetic Field Laboratory (HLD-EMFL), Helmholtz-Zentrum Dresden-Rossendorf, 01328 Dresden, Germany

<sup>3</sup>Leibniz Institute for Solid State and Materials Research (IFW) Dresden, 01069 Dresden, Germany

<sup>4</sup>Institute of Natural Sciences and Mathematic, Ural Federal University, Yekaterinburg 620075, Russia

<sup>5</sup>Dresden Center for Nanoanalysis (DCN), Center for Advancing Electronics Dresden (cfaed), TU Dresden, 01062 Dresden, Germany

<sup>6</sup>Max Planck Institute of Microstructure Physics, Weinberg 2, 06120 Halle, Germany

<sup>7</sup>Institute for Materials Science, TU Dresden, 01062 Dresden, Germany



(Received 25 October 2021; accepted 3 February 2022; published 18 February 2022)

The increasing demand for computer data storage with a higher recording density can be addressed by using smaller magnetic objects, such as bubble domains. Small bubbles predominantly require a strong saturation magnetization combined with a large magnetocrystalline anisotropy to resist self-demagnetization. These conditions are well satisfied for highly anisotropic materials. Here, we study the domain structure of thin Nd<sub>2</sub>Fe<sub>14</sub>B lamellae. Magnetic bubbles with a minimum diameter of 74 nm were observed at room temperature, approaching even the range of magnetic skyrmions. The stripe domain width and the bubble size are both thickness dependent. Furthermore, a kind of bubble was observed below the spin-reorientation transition temperature that combine bubbles with opposite helicity. In this paper, we reveal Nd<sub>2</sub>Fe<sub>14</sub>B to be a good candidate for a high-density magnetic bubble-based memory.

DOI: [10.1103/PhysRevB.105.064426](https://doi.org/10.1103/PhysRevB.105.064426)

### I. INTRODUCTION

Magnetic bubbles are small magnetized cylindrical volumes in magnetic films with uniaxial, perpendicular magnetocrystalline anisotropy that can be used for computer data storage [1]. Magnetic bubbles were extensively studied from the 1960s to the 1970s, finally culminating in the highly sophisticated magnetic bubble memory that was introduced in the 1970s. At that time, the focus was on oxides that include rare-earth iron garnets, orthoferrites, and hexaferrites [2]. These materials exhibit magnetic bubbles with typical diameters in the 1–100 μm range. Unfortunately, owing to the large size, bubble memory cannot compete with semiconductor memories with a bit size of ~30 nm. The need for smaller bubbles for commercial applications led to the recent introduction of the concept of skyrmions [3,4].

Compared with skyrmions, the diameter (usually 1–100 nm) of which mainly depends on the Dzyaloshinskii-Moriya interaction, the diameter of bubbles depends on both the intrinsic and extrinsic properties such as anisotropy, saturation magnetization, and the film thickness [2]. The diameter

$d$  of a bubble reaches a minimum for  $d = h$  [2,5,6] when the thickness  $h$  satisfies the condition:

$$h = \frac{16\sqrt{AK_1}}{\mu_0 M_s^2}, \quad (1)$$

where  $A$  is the exchange stiffness constant,  $K_1$  is the magnetocrystalline anisotropy,  $\mu_0$  is the vacuum permeability, and  $M_s$  is the saturation magnetization. Detailed analysis can be found in the Appendix. Although a small uniaxial magnetic anisotropy  $K_1$  is favorable for decreasing the diameter, a large  $K_1$  is required to resist the self-demagnetization of lamellae or films, which requires  $K_1 > \frac{1}{2}\mu_0 M_s^2$ . Therefore, obtaining small bubbles dominantly requires strong  $M_s$  [7] in combination with relatively high  $K_1$ . Conventional materials for obtaining bubbles were ferrimagnetic (garnets and hexaferrites) or canted antiferromagnetic (orthoferrites); therefore, bubbles were large because of the low  $M_s$ .

A similar combination of large anisotropy and saturation magnetization is also required for permanent magnets. A good hard magnet fulfills  $K_1 > \mu_0 M_s^2$  [8]; therefore, magnetic bubbles can be found in all highly anisotropic materials when prepared in a form of thin lamellae or film. Moreover, due to the large  $M_s$ , the bubbles in hard magnets can be rather small. In fact, the existence of small bubbles in hard magnetic barium ferrite [9], L1<sub>0</sub> Fe-Pt [10], and MnBi [11] with diameters of 130, 150, and 160 nm, respectively, at room temperature has already been confirmed.

Materials based on the Nd<sub>2</sub>Fe<sub>14</sub>B compound with tetragonal crystal structure are used for permanent magnets with the

\*yangkun.he@cpfs.mpg.de

largest energy product. This material has a high Curie temperature of  $T_c = 588$  K and large magnetocrystalline anisotropy of  $K_1 = 4.9$  MJm $^{-3}$  at room temperature [12], which is sufficiently strong to resist self-demagnetization. The ferromagnetically coupled moments of Nd and Fe become noncollinear below the spin-reorientation transition temperature  $T_{SR} = 135$  K, and the net moment is gradually tilted away from the  $c$  axis, forming an easy-cone spin structure at low temperatures [13]. As a well-known material, most of the previous studies were focused on the magnetic properties of the bulk material at room temperature. However, less attention has been paid to the domain structure of mesoscopic sized crystals or films, and studies of the domains in films or lamellae below  $T_{SR}$  have not yet been well reported. At room temperature in mesoscopic samples, such as thin lamellae, the competition between minimizing the domain wall energy and the dipolar interaction [9] leads to a stripe domain structure [14] rather than the two-phase two-branched pattern (star-like/mazelike) that occurs in the bulk material [5,13]. These stripe domains (sometimes classified as band domains [5]) are the ground state for skyrmions or bubbles, which are stabilized by an applied magnetic field. The saturation magnetization of Nd $_2$ Fe $_{14}$ B at room temperature ( $\mu_0 M_s = 1.6$  T) is the largest among all hard magnets, providing a good opportunity for bubble memory with a small bit (domain) size.

In this paper, we present our study of the domain structure of thin Nd $_2$ Fe $_{14}$ B lamellae using magneto-optical Kerr microscopy and Lorentz transmission electron microscopy (L-TEM). Magnetic bubbles with a minimum diameter of 74 nm were observed at room temperature, even comparable with the size of magnetic skyrmions. A type of bubble spin structure was observed below  $T_{SR}$ .

## II. EXPERIMENTAL DETAILS

### A. Single-crystal characterization

Single crystals of Nd $_2$ Fe $_{14}$ B were purchased from MaTeck, Jülich, Germany. The composition was characterized by wavelength dispersive x-ray spectroscopy as Nd $_2$ Fe $_{14}$ B with an uncertainty of  $\sim 0.5\%$ . The orientation of the single crystals was confirmed using the Laue method.

### B. Preparation of micron-sized transport devices

Thin lamellae of Nd $_2$ Fe $_{14}$ B were cut using a focused ion beam (FIB). The sample size was  $80.00$  (aaxis)  $\times$   $3.5$  (baxis)  $\mu\text{m}^2$ . The thickness varies from  $2.4$  to  $13$   $\mu\text{m}$  along the  $c$  axis. The lamellae were affixed to sapphire substrates using epoxy and gold contacts that were deposited via sputtering.

### C. Magnetization measurements

The magnetic properties of the single crystals were measured using a vibrating sample magnetometer (MPMS 3, Quantum Design). An empty sample holder containing only the substrate and epoxy was measured for comparison to remove the diamagnetic background. The mass was calculated using the volume of the sample.

### D. Magneto-optical Kerr microscopy

Domain images were obtained using the polar Kerr effect in a wide-field magneto-optical Kerr microscope [15,16] at room temperature on a (001) surface.

### E. L-TEM

The magnetic phases were imaged with a double-corrected FEI Titan $^3$  80–300 and a JEOL Jem F-200C transmission electron microscope operated in Lorentz mode at an acceleration voltage of 300 and 200 kV, respectively. The sample was maintained at the required temperature using liquid nitrogen in a Gatan double-tilt cooling holder.

## III. RESULTS

The evolution of domain structure of a thin Nd $_2$ Fe $_{14}$ B lamella with a (001) surface in the presence of a magnetic field applied parallel to the  $c$  axis at room temperature is shown in Fig. 1. The thickness of the sample is  $2$   $\mu\text{m}$ ; therefore, the competition between ferromagnetic exchange, wall energy, and dipole-dipole interaction changes the domain pattern from that of two-phase branched domains in bulk samples to that of stripe domains in thin lamellae without an applied magnetic field [see Panel A of Fig. 1(a)]. When the magnetic field becomes stronger, the darker domain phase parallel to the magnetic field expands, and the brighter domain phase antiparallel to the magnetic field shrinks (see Panels B and C). A further increase in the field has the effect of transforming the stripe domains into individual bubbles (Panels D–F) before the magnetization finally saturates (Panel G). During the demagnetization process, the single-domain state remains until the sudden appearance of stripe domains in Panel I. The magnetic field corresponding to the domain pattern in Panels A–I can be taken from the plot in Fig. 1(b).

The high-resolution observation of the stripe domains and magnetic bubbles was also performed using L-TEM, as shown in Fig. 2. The images in Figs. 2(a)–2(d) were captured from a 250-nm-thick sample, whereas the inset of Fig. 2(a) and Figs. 2(e) and 2(f) are taken from a sample with 90 nm thickness. The magnetization inside the stripes is opposite to that of the applied magnetic field. The domain wall is a Bloch type, where the moment lies in plane. The Bloch lines that arise when wall segments with an opposite rotation sense meet are indicated by yellow arrows, wherein the gray level of the domain wall in the images changes between dark and light. A schematic of the domain structure and zoomed image of the stripes at 0.8 T, marked by the dashed box in Fig. 2(b), are shown in Fig. 2(c). The individual bubbles become smaller with increasing magnetic field, and the diameter shrinks from 300 nm at 0.95 T to  $>180$  nm at 1.04 T in the 250-nm-thick sample. Using the transport-of-intensity equation (TIE) [17], the magnetic bubbles are identified as type II [18], with Bloch lines in the Bloch wall in Fig. 2(f). The Bloch line indicates an in-plane component of the moment, which might be because the sample is slightly tilted ( $\sim 3^\circ$  out of the [001] zone axis) to reduce dynamical diffraction in the L-TEM experiments. Interestingly, the topological Hall effect was also observed in the thin lamella without tilting. The value of the topological Hall angle is like that raised by skyrmions [19,20]. Detailed

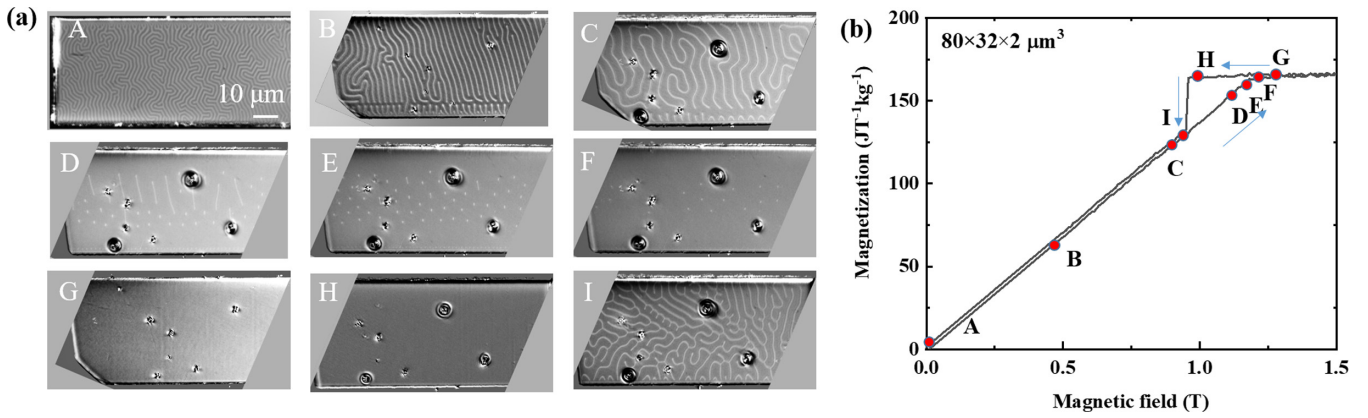


FIG. 1. (a) Kerr microscopy images: domain structure of a thin lamella of Nd<sub>2</sub>Fe<sub>14</sub>B (2 μm thick), observed by Kerr microscopy on the (001) surface with a magnetic field applied parallel to the *c* axis (perpendicular to the observed plane) at room temperature. The magnetic fields corresponding to the domain patterns in A–I can be taken from the plot in (b). (b) Magnetization curve in a thin lamella of Nd<sub>2</sub>Fe<sub>14</sub>B.

data can be found in the Supplemental Material [21]. However, since type-II bubbles are topologically trivial and should not give rise to any topological Hall effect, it remains an open question whether the bubbles are chiral with the field applied along the *c* axis. It might be possible that type-II bubbles transfer to type-I bubbles when the tilt is removed [9].

The period of the stripe domains in zero field and the minimum diameter of the bubbles near the collapse field are strongly dependent on the thickness. A decrease in the thickness from 250 to 90 nm is accompanied by a decrease in the periodicity λ from 360 to 120 nm. Reportedly, even a periodicity of 30 nm was observed in a 10-nm-thick L-TEM sample

edge [14]. In addition, the minimum diameter of the bubble decreases from 180 nm in the 250-nm-thick sample to ~74 nm in a sample with a thickness of 90 nm. In theory, a minimum diameter of 50 nm can be realized in a 50-nm-thick sample, calculated using Eq. (1) (see Discussion and Appendix).

To study the thickness dependence of the domain structure further, a wedge-shaped sample with a thickness ranging from 2.4 to 13.7 μm was prepared. The thickness-dependent domain structures are shown in Fig. 3. As the thickness increases, the width of the stripe domains gradually increases from 0.9 to 3.5 μm at zero field, as shown in Fig. 3(b). The trend follows that the width is proportion to the root of the thickness [5], as summarized in Fig. 3(d). In an applied

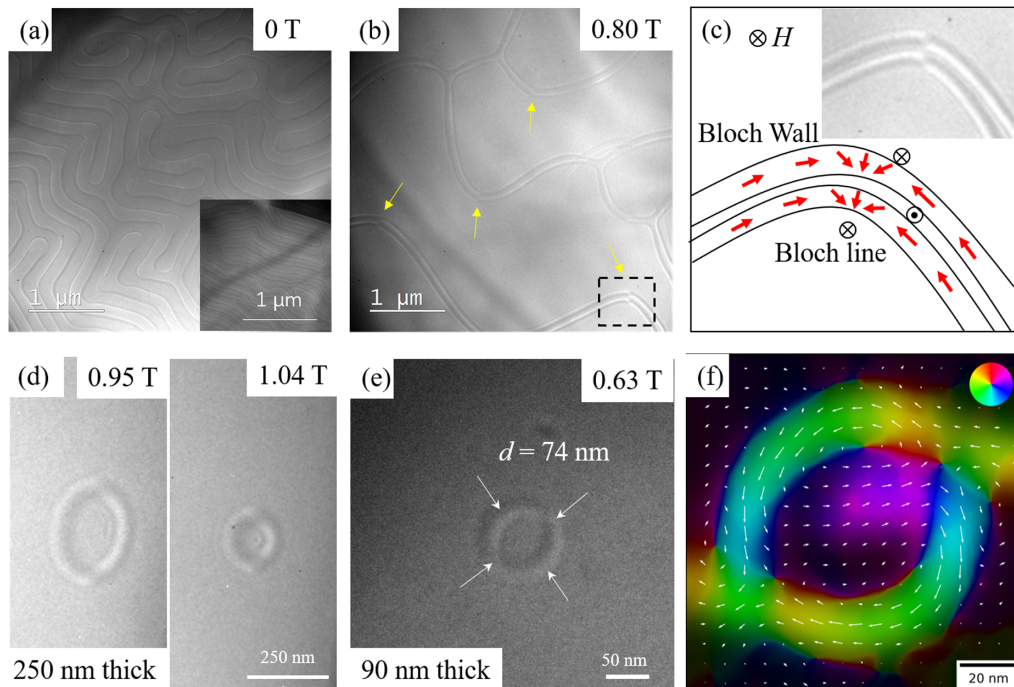


FIG. 2. Domain structure of stripe and magnetic bubbles observed by Lorentz transmission electron microscopy (L-TEM) at room temperature. (a)  $\mu_0 H = 0$  T. (b)  $\mu_0 H = 0.8$  T. (c) Enlargement of the box in (b). (d) Individual bubbles at 0.95 and 1.04 T in a sample that is 250 nm thick. (e) Bubble at 0.63 T in a 90-nm-thick sample. (f) Direction of the projected in-plane magnetic induction reconstructed by the transport-of-intensity equation (TIE).



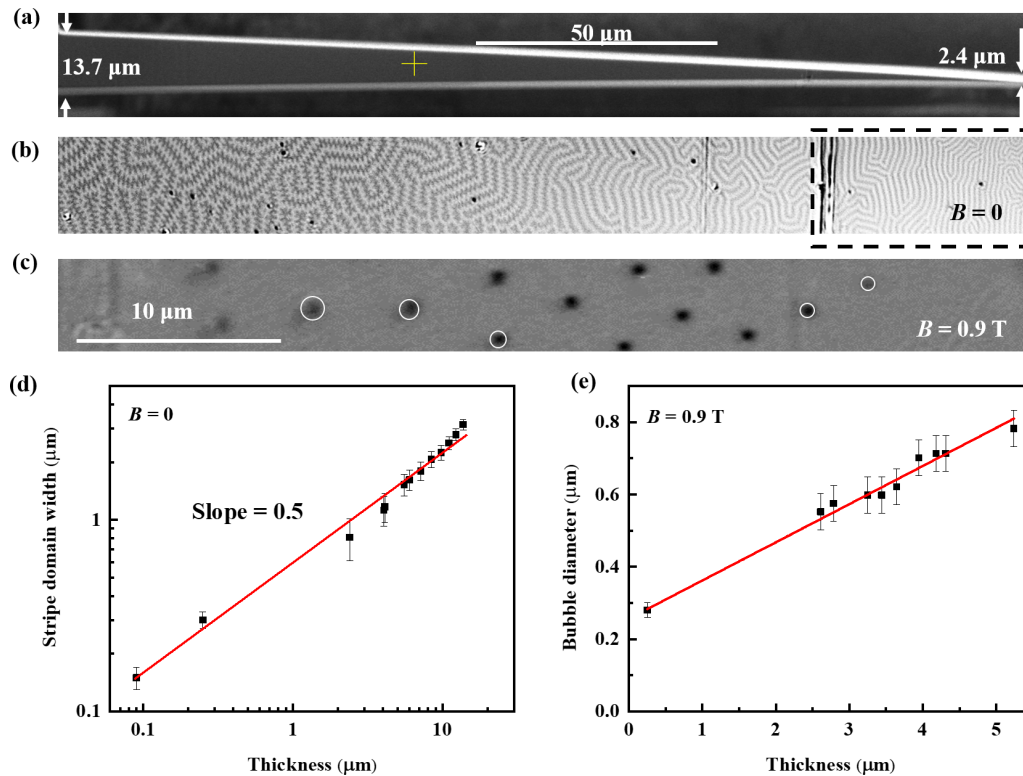


FIG. 3. Thickness-dependent domain structure. (a) Wedge-shaped thin lamella viewed from the side. (b) Domain structure as seen from the top of the wedge from [001]. (c) Domain structure from the area demarcated by the box in (b) in an applied magnetic field of 0.9 T. Some of the bubbles are marked by white circles to show their size. (d) Dependence of the stripe domain width on thickness. (e) Dependence of the bubble diameter at 0.9 T on thickness.

magnetic field of 0.9 T, the diameter of the bubbles also increases from 0.55 to 0.75  $\mu\text{m}$  as the thickness increases from 2.4 to 5.7  $\mu\text{m}$ , as shown in Fig. 3(c) and 3(e). It is worth mentioning that the strip domain starts to change its shape toward branching when the thickness is  $>6.2 \mu\text{m}$  [Fig. 3(b)], which is also the critical boundary between the bulk and the mesoscale thin lamella. To reduce the stray field provided by the large stripe domain [5], surface domain modification (branching) starts to appear at the cost of an additional domain wall energy on the condition that  $D/(Q\sqrt{A/K_u}) = 10^3$ , where  $D$  is the thickness,  $Q$  is the quality factor  $Q = 2K_u/(\mu_0 M_s^2)$ , and  $A$  is the exchange constant that can be estimated from its Curie temperature. The values at room temperature are  $Q = 4.5$ ,  $K_u = 4.9 \text{ MJm}^{-3}$ , and  $A = 8 \text{ pJm}^{-1}$  [12]. Therefore, the critical thickness  $D$  is  $\sim 6 \mu\text{m}$ , which agrees well with our experiment.

At temperatures below  $T_{\text{SR}} = 135 \text{ K}$ ,  $\text{Nd}_2\text{Fe}_{14}\text{B}$  has an easy-cone-type noncollinear spin structure. The domain structure at low temperatures was observed by L-TEM (see Fig. 4). Compared with the domain structure in Fig. 3(a), additional lines exist that are perpendicular to the stripes in the ground state, as indicated by the arrows. A schematic of the domain structure is shown in Fig. 4(c). These lines are  $90^\circ$  domain walls, which separate two domains in a head-to-head way. This domain structure is forbidden in soft magnetic materials, but the strong magnetocrystalline anisotropy owing to Nd forces the moments to be aligned along the easy direction

rather than along the  $c$  axis. Nonetheless, a large component of the magnetic moment remains along the  $c$  axis; therefore, the stripe domains still exist.

In an applied magnetic field, the  $90^\circ$  domain walls quickly vanish [Fig. 4(b)] alongside the shrink of these stripes. Finally, stripe domains break into bubbles. However, the spin texture of this contrast is definitely different from either type-I or II bubbles. Additional tails remain, which point in the easy direction, marked by the yellow arrows. The projected in-plane magnetic induction map shows that it is like a combination of a type-I and a type-II bubble in Fig. 4(f) rather than simple bubbles in a previous study [22]. The detailed magnetic structure of this kind of domain combined with a tail remains to be elucidated. More measurements are required to properly understand its nature.

The size and helicity of skyrmions are mainly determined by the Dzyaloshinskii-Moriya interactions and the crystal structure. However, a unique feature of magnetic bubbles is that their topological charge and size can be controlled by the thickness of the sample and an external magnetic field. Here, we further demonstrate that the magnetocrystalline anisotropy itself can influence the bubble structure.

We also observe a topological Hall effect at low temperatures below  $T_{\text{SR}}$  in the bulk material (see Fig. S5 in the Supplemental Material [21]). However, this effect is due to the noncoplanar spin structure of Nd and Fe rather than any topological domain structure in the thin lamellae.

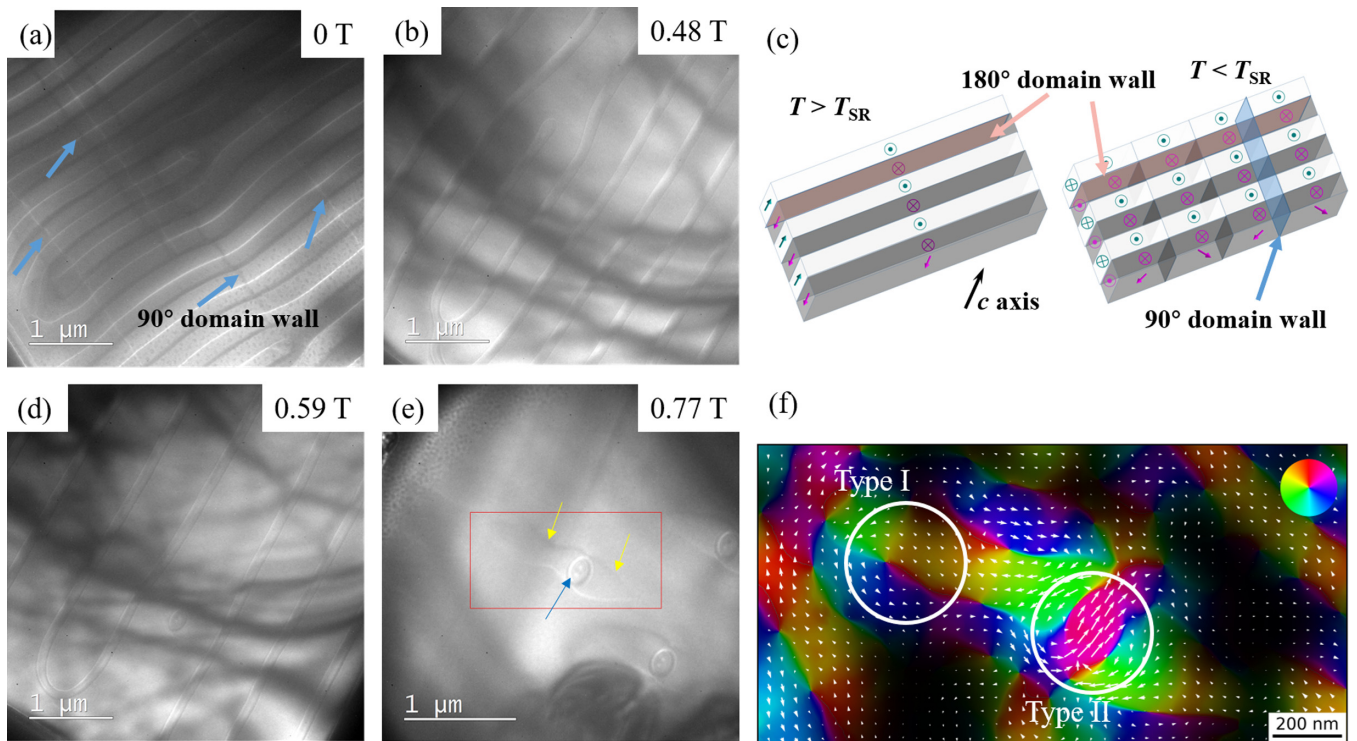


FIG. 4. Domain structure below the spin-reorientation transition temperature at 110 K. (a) Domain structure in the absence of a magnetic field. (b) Domain structure at 0.48 T without 90° domain wall. (c) Schematic view of the domain structure above (left) and below (right)  $T_{SR}$  at zero magnetic field. Additional 90° domain wall appears below  $T_{SR}$ . (d) Domain structure at 0.59 T with individual bubbles starting to form. (e) Bubbles with two cores inside and a tail extending in the easy direction. (f) Direction of the projected in-plane magnetic induction from the area inside the red box in (e).

#### IV. DISCUSSION

In Figs. 5(a) and 5(b), the phase diagrams of Nd<sub>2</sub>Fe<sub>14</sub>B in the bulk form as well as thin lamellae are compared for field applied along the  $c$  axis. The phase boundaries for the bulk are obtained from the field-dependent susceptibility from the magnetization curves shown in Fig. S3 in the Supplemental Material [21], while those for thin lamella are obtained from the microscopic domain images. The bulk sample has a uniaxial easy-axis magnetic structure  $>135$  K and an easy-cone structure below. In the latter phase, the cone angle shrinks in the presence of an applied magnetic field  $>1$  T. However, for a thin lamella, the competition between the wall energy, exchange, and dipole-dipole interaction, which is between that of short- and long-range order, leads to stripe domains and bubbles. Below the spin-reorientation transition temperature, a stripe domain with an additional 90° domain wall appears, which transforms into complex bubbles in an applied magnetic field.

The minimum bubble size observed in Nd<sub>2</sub>Fe<sub>14</sub>B is one of the smallest that has been found yet in all skyrmion and bubble materials at room temperature [see the compilation in Fig. 5(c)], owing to the large saturation magnetization of this material. This value is also comparable with that of certain multilayer film systems, which have diameters in the  $<100$  nm range [23–27]. To further decrease the bubble diameter, it is desirable to slightly decrease  $K_1$  while maintaining its easy-axis magnetization, according to Eq. (1).

Based on the intrinsic magnetic properties at room temperature [28] and calculation using Eq. (1), we predict that, among all  $R_2T_{14}B$  compounds ( $R$  = rare earth or Th,  $T$  = Fe and Co), the theoretical minimum diameter of bubbles in La<sub>2</sub>Fe<sub>14</sub>B can be as small as 30 nm because of the much smaller  $K_1$ , which is even smaller than the 50 nm in Nd<sub>2</sub>Fe<sub>14</sub>B. The minimum diameter can be further decreased in alloys with partial substitution of Nd by Sm, or Fe by Co, to lower  $K_1$  while maintaining a strong  $M_s$  and still large enough to resist self-demagnetization. In this case, the theoretical minimum diameter for a (Nd, Sm)<sub>2</sub>Fe<sub>14</sub>B alloy could be as small as 25 nm (see Table I). Despite the drawback of a high magnetic field ( $\sim 1$  T) to obtain the bubbles, the small size is promising to increase the magnetic recording density.

#### V. SUMMARY

In summary, we report the existence of magnetic bubbles in Nd<sub>2</sub>Fe<sub>14</sub>B. The experimentally observed minimum diameter of 74 nm at room temperature is one of the smallest among all reported materials owing to the large saturation magnetization of Nd<sub>2</sub>Fe<sub>14</sub>B. The domain structure depends on both the magnetic field and the thickness. Below the spin-reorientation transition, stripe domains with additional 90° domain walls appear owing to the in-plane anisotropy, and they are transformed into complex bubbles upon application of a magnetic field. In this paper, we not only shed light on Nd<sub>2</sub>Fe<sub>14</sub>B, but the results are also applicable to other hard magnetic materials. Unlike many skyrmion materials with low magnetic ordering temperatures, several well-known hard magnets have

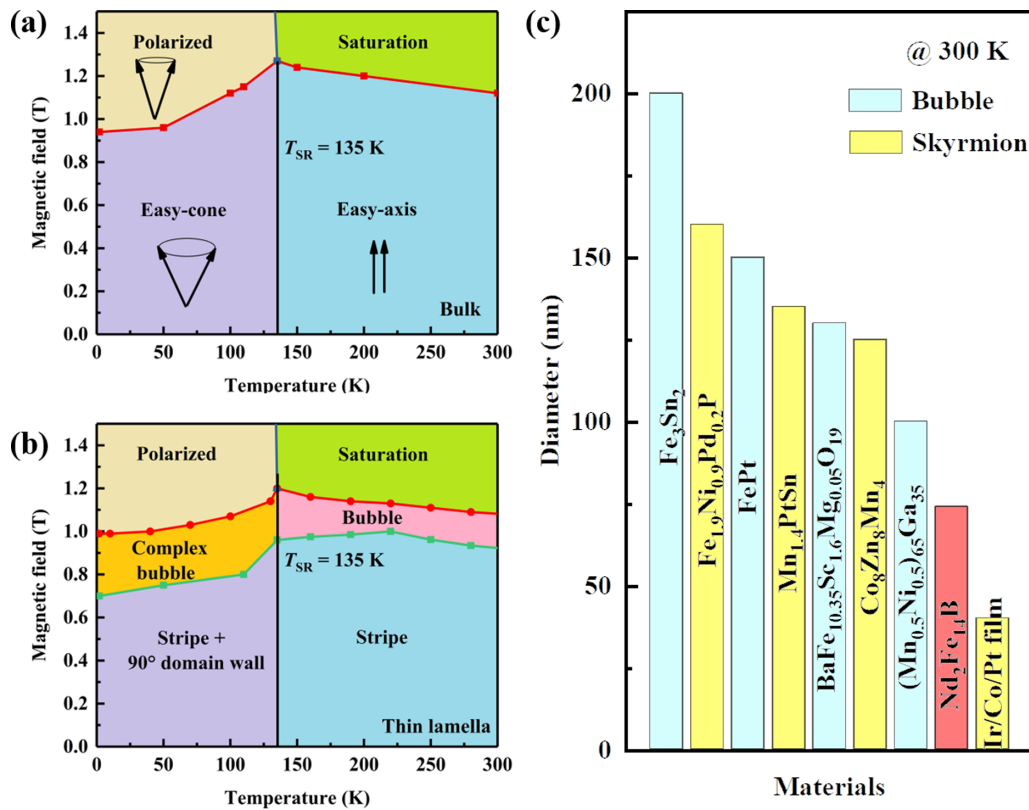


FIG. 5. Phase diagram for (a) bulk and (b) thin lamella  $\text{Nd}_2\text{Fe}_{14}\text{B}$ . (c) Minimum observed diameter of skyrmions or bubbles at room temperature compiled from previous reports [9,10,27,29–33].

a high Curie temperature and strong magnetization, which are promising for applications.

TABLE I. Room temperature magnetic properties and minimum bubble diameter. The magnetic properties were taken from Ref. [28].  $\text{Sm}_2\text{Fe}_{14}\text{B}$ ,  $\text{Er}_2\text{Fe}_{14}\text{B}$ ,  $\text{Tm}_2\text{Fe}_{14}\text{B}$ , and  $\text{Yb}_2\text{Fe}_{14}\text{B}$  have easy-plane spin structures at room temperature. Here,  $H_a$  is the anisotropy field, and to satisfy the condition for bubble stabilization,  $K_1 > \frac{1}{2}\mu_0 M_s^2$ ,  $H_a > M_s$ .

	Moment ( $\mu_B/\text{f.u.}$ )	$\mu_0 H_a$ (T)	$T_c$ (K)	$d$ (nm)
$\text{Y}_2\text{Fe}_{14}\text{B}$	26.8	2.3	566	37
$\text{La}_2\text{Fe}_{14}\text{B}$	28.6	2	543	30
$\text{Ce}_2\text{Fe}_{14}\text{B}$	22.9	3.5	529	56
$\text{Pr}_2\text{Fe}_{14}\text{B}$	31.9	8	567	53
$\text{Nd}_2\text{Fe}_{14}\text{B}$	32.5	7	588	49
$\text{Sm}_2\text{Fe}_{14}\text{B}$	30.2	–	622	–
$\text{Gd}_2\text{Fe}_{14}\text{B}$	17.5	2.5	659	78
$\text{Tb}_2\text{Fe}_{14}\text{B}$	14	22	623	316
$\text{Dy}_2\text{Fe}_{14}\text{B}$	14	15	592	255
$\text{Ho}_2\text{Fe}_{14}\text{B}$	15.9	8	570	151
$\text{Er}_2\text{Fe}_{14}\text{B}$	17.7	–	551	–
$\text{Tm}_2\text{Fe}_{14}\text{B}$	22.6	–	544	–
$\text{Yb}_2\text{Fe}_{14}\text{B}$	23	–	525	–
$\text{Lu}_2\text{Fe}_{14}\text{B}$	22.7	2.6	541	49
$\text{Th}_2\text{Fe}_{14}\text{B}$	25.9	2	480	33
$\text{Pr}_2\text{Co}_{14}\text{B}$	23	14	995	151
$\text{Nd}_2\text{Co}_{14}\text{B}$	23	5	1007	91
$(\text{Nd, Sm})_2\text{Fe}_{14}\text{B}$	31	1.6	600	25

## ACKNOWLEDGMENTS

This paper was financially supported by an Advanced Grant from the European Research Council (No. 742068) “TOPMAT,” the European Union’s Horizon 2020 research and innovation program (No. 824123) “SKYTOP,” the European Union’s Horizon 2020 research and innovation program (No. 766566) “ASPIN,” the Deutsche Forschungsgemeinschaft (Project-ID 258499086) “SFB 1143,” the Deutsche Forschungsgemeinschaft (DFG; Project-IDs FE 633/30-1, RE 1164/6-1, and LU 2261/2-1) “SPP Skyrmionics,” the DFG through the Würzburg-Dresden Cluster of Excellence on Complexity and Topology in Quantum Matter ct.qmat (EXC 2147, Project-ID 39085490). I.S. would like to express his gratitude to the DFG for supporting this paper through Project SO 1623/2-1.

The characterization of the single crystals and the magnetic and transport measurements were performed by Y.H. with the help of W.S. The L-TEM was performed by S.S., D.P., A. K. Srivastava, A. K. Sharma, and B.R. The FIB microstructure transport devices were fabricated by T. H. Kerr microscopy images were taken by I.S. and R.S. All the authors discussed the results. The paper was written by Y.H. and G.H.F., with feedback from all the authors. The project was supervised by C.F.

The authors declare no competing financial interests.

## APPENDIX

For a uniaxial system, the minimum diameter  $d$  of the bubble is reached when the thickness  $h$  satisfies the condition

[2,5]:

$$h = 4l. \tag{A1}$$

Here,  $l$  is the characteristic length, which can be expressed by

$$l = \frac{\sigma_w}{M_s^2}, \tag{A2}$$

where  $\sigma_w$  is the domain wall energy density,  $\mu_0$  is the vacuum permeability, and  $M_s$  is the saturation magnetization. The domain wall energy density  $\sigma_w = 4\sqrt{AK_1}$ , where  $A$  and  $K_1$  are the exchange stiffness and the magnetocrystalline anisotropy, respectively. Therefore,

$$h = \frac{16\sqrt{AK_1}}{\mu_0 M_s^2}. \tag{A3}$$

The minimum diameter  $d$  is equal to the thickness  $h$ .

In Nd<sub>2</sub>Fe<sub>14</sub>B at room temperature, the domain wall energy density is  $\gamma_w = 25 \times 10^{-3} \text{Jm}^{-2}$  and using  $A = 8 \text{pJm}^{-1}$ ,  $K_1 = 4.9 \text{MJm}^{-3}$ , and  $\mu_0 M_s = 1.6 T^{12}$ , our calculation determined that  $h = d = 48 \text{nm}$ . For other  $R_2T_{14}B$  compounds ( $R = \text{rare-earth element}$ ,  $T = \text{Fe and Co}$ ), the theoretical minimum diameter of the bubbles was calculated similarly. The exchange stiffness  $A$  was estimated according to the Curie temperature compared with Nd<sub>2</sub>Fe<sub>14</sub>B.

In La<sub>2</sub>Fe<sub>14</sub>B, the minimum  $d$  can be as small as 30 nm, which is even smaller than that of 50 nm for Nd<sub>2</sub>Fe<sub>14</sub>B. The decrease in size is mainly owing to the reduced  $K_1$  in the absence of magnetic rare-earth elements. The minimum diameter can be further decreased by alloying Nd with Sm or Fe with Co to obtain  $K_1 = \frac{1}{2}\mu_0 M_s^2$  while maintaining the large  $M_s$ . In this case, the theoretical minimum diameter for the (Nd, Sm)<sub>2</sub>Fe<sub>14</sub>B alloy could be as small as 25 nm.

---

[1] A. H. Bobeck and H. E. D. Scovil, Magnetic bubbles, *Sci. Am.* **224**, 78 (1971).

[2] A. H. Bobeck, P. I. Bonyhard, and J. E. Geusic, Magnetic bubbles—an emerging new memory technology, *Proc. IEEE* **63**, 1176 (1975).

[3] N. Kanazawa, S. Seki, and Y. Tokura, Noncentrosymmetric magnets hosting magnetic skyrmions, *Adv. Mater.* **29**, 1603227 (2017).

[4] N. S. Kiselev, A. N. Bogdanov, R. Schäfer, and U. K. Rößler, Chiral skyrmions in thin magnetic films: new objects for magnetic storage technologies? *J. Phys. D: Appl. Phys.* **44**, 392001 (2011).

[5] A. Hubert and R. Schäfer, *Magnetic Domains* (Springer, Berlin, 1998), Chap. 3.

[6] A. A. Thiele, The theory of cylindrical magnetic domains, *Bell Syst. Tech. J.* **48**, 3287 (1969).

[7] E. A. Giess, Magnetic bubble materials, *Science* **208**, 938 (1980).

[8] R. Skomski and J. M. D. Coey, Magnetic anisotropy—how much is enough for a permanent magnet? *Script. Mater.* **112**, 3 (2016).

[9] X. Yu, M. Mostovoy, Y. Tokunaga, W. Zhang, K. Kimoto, Y. Matsui, Y. Kaneko, N. Nagaosa, and Y. Tokura, Magnetic stripes and skyrmions with helicity reversals, *Proc. Natl. Acad. Sci. USA* **109**, 8856 (2012).

[10] C. Moutafis, S. Komineas, C. A. F. Vaz, J. A. C. Bland, T. Shima, T. Seki, and K. Takanashi, Magnetic bubbles in FePt nanodots with perpendicular anisotropy, *Phys. Rev. B* **76**, 104426 (2007).

[11] Y. He, S. Schneider, T. Helm, J. Gayles, D. Wolf, and I. Soldatov, Topological Hall effect arising from the mesoscopic and microscopic non-coplanar magnetic structure in MnBi, *Acta Mater.* **226**, 117619 (2022).

[12] J. M. D. Coey, *Magnetism and Magnetic Materials* (Cambridge University Press, Cambridge, 2010).

[13] Y. G. Pastushenkov, A. Forkl, and H. Kronmüller, Temperature dependence of the domain structure in Fe<sub>14</sub>Nd<sub>2</sub>B single crystals during the spin-reorientation transition, *J. Magn. Magn. Mater.* **174**, 278 (1997).

[14] Y. Zhu and M. R. McCartney, Magnetic-domain structure of Nd<sub>2</sub>Fe<sub>14</sub>B permanent magnets, *J. Appl. Phys.* **84**, 3267 (1998).

[15] I. V. Soldatov and R. Schäfer, Selective sensitivity in Kerr microscopy, *Rev. Sci. Instrum.* **88**, 073701 (2017).

[16] I. V. Soldatov and R. Schäfer, Advanced MOKE magnetometry in wide-field Kerr-microscopy, *J. Appl. Phys.* **122**, 153906 (2017).

[17] V. V. Volkov and Y. Zhu, Lorentz phase microscopy of magnetic materials, *Ultramicroscopy* **98**, 271 (2004).

[18] J. C. Loudon, A. C. Twitchett-Harrison, D. Cortés-Ortuño, M. T. Birch, L. A. Turnbull, A. Štefančič, F. Y. Ogrin, E. O. Burgos-Parra, N. Bukin, A. Laurenson, H. Popescu, M. Beg, O. Hovorka, H. Fangohr, P. A. Midgley, G. Balakrishnan, and P. D. Hatton, Do images of biskyrmions show type-II bubbles? *Adv. Mater.* **31**, 1806598 (2019).

[19] L. Vistoli, W. Wang, A. Sander, Q. Zhu, B. Casals, R. Cichelero, A. Barthélémy, S. Fusil, G. Herranz, S. Valencia, R. Abrudan, E. Weschke, K. Nakazawa, H. Kohno, J. Santamaria, W. Wu, V. Garcia, and M. Bibes, Giant topological Hall effect in correlated oxide thin films, *Nat. Phys.* **15**, 67 (2019).

[20] K. Zeissler, S. Finizio, K. Shahbazi, J. Massey, F. A. Ma’Mari, D. M. Bracher, A. Kleibert, M. C. Rosamond, E. H. Linfield, T. A. Moore, J. Raabe, G. Burnell, and C. H. Marrows, Discrete Hall resistivity contribution from Néel skyrmions in multilayer nanodiscs, *Nature Nano* **13**, 1161 (2018).

[21] See Supplemental Material at <http://link.aps.org/supplemental/10.1103/PhysRevB.105.064426> for details of magnetization curves of a thin lamella, magnetic domain for bulk sintered magnet, magnetic properties of bulk single crystal, resistivity and magnetoresistivity, Hall resistivity of bulk single crystals and topological Hall effect on thin lamella.

[22] Y. Xiao, F. J. Morvan, A. N. He, M. K. Wang, H. B. Luo, R. B. Jiao, W. X. Xia, G. P. Zhao, and J. P. Liu, Spin-reorientation transition induced magnetic skyrmion in Nd<sub>2</sub>Fe<sub>14</sub>B magnet, *Appl. Phys. Lett.* **117**, 132402 (2020).

[23] C. Moreau-Luchaire, C. Moutafis, N. Reyren, J. Sampaio, C. A. F. Vaz, N. Van Horne, K. Bouzehouane, K. Garcia, C. Deranlot, P. Warnicke, P. Wohlhüter, J.-M. George, M. Weigand, J. Raabe,



- V. Cros, and A. Fert, Additive interfacial chiral interaction in multilayers for stabilization of small individual skyrmions at room temperature, *Nat. Nanotechnol.* **11**, 444 (2016).
- [24] O. Boulle, J. Vogel, H. Yang, S. Pizzini, D. de Souza Chaves, A. Locatelli, T. O. Mentes, A. Sala, L. D. Buda-Prejbeanu, O. Klein, M. Belmeguenai, Y. Roussigné, A. Stashkevich, S. M. Chérif, L. Aballe, M. Foerster, M. Chshiev, S. Auffret, I. M. Miron, and G. Gaudin, Room-temperature chiral magnetic skyrmions in ultrathin magnetic nanostructures, *Nat. Nanotechnol.* **11**, 449 (2016).
- [25] S. Woo, K. Litzius, B. Krüger, M. Y. Im, L. Caretta, K. Richter, M. Mann, A. Krone, R. M. Reeve, M. Weigand, P. Agrawal, I. Lemesh, M.-A. Mawass, P. Fischer, M. Kläui, and G. S. D. Beach, Observation of room-temperature magnetic skyrmions and their current-driven dynamics in ultrathin metallic ferromagnets, *Nat. Mater.* **15**, 501 (2016).
- [26] W. Legrand, D. Maccariello, F. Ajejas, S. Collin, A. Vecchiola, K. Bouzehouane, N. Reyren, V. Cros, and A. Fert, Room-temperature stabilization of antiferromagnetic skyrmions in synthetic antiferromagnets, *Nat. Mater.* **19**, 34 (2020).
- [27] A. Soumyanarayanan, M. Raju, A. L. Gonzalez Oyarce, A. K. C. Tan, M. Im, A. P. Petrovic, P. Ho, K. H. Khoo, M. Tran, C. K. Gan, F. Ernult, and C. Panagopoulos, Tunable room-temperature magnetic skyrmions in Ir/Fe/Co/Pt multilayers, *Nat. Mater.* **16**, 898 (2017).
- [28] J. M. D. Coey, Intrinsic magnetic properties of compounds with the  $\text{Nd}_2\text{Fe}_{14}\text{B}$  structure, *J. Less Common Met.* **126**, 21 (1986).
- [29] Z. Hou, W. Ren, B. Ding, G. Xu, Y. Wang, B. Yang, Q. Zhang, Y. Zhang, E. Liu, F. Xu, W. Wang, G. Wu, X. Zhang, B. Shen, and Z. Zhang, Observation of various and spontaneous magnetic skyrmionic bubbles at room temperature in a frustrated kagome magnet with uniaxial magnetic anisotropy, *Adv. Mater.* **29**, 1701144 (2017).
- [30] W. Wang, Y. Zhang, G. Xu, L. Peng, B. Ding, Y. Wang, Z. Hou, X. Zhang, X. Li, E. Liu, S. Wang, J. Cai, F. Wang, J. Li, F. Hu, G. Wu, B. Shen, and X.-X. Zhang, A centrosymmetric hexagonal magnet with superstable biskyrmion magnetic nanodomains in a wide temperature range of 100–340 K, *Adv. Mater.* **28**, 6887 (2016).
- [31] A. K. Nayak, V. Kumar, T. Ma, P. Werner, E. Pippel, R. Sahoo, F. Damay, U. K. Röbler, C. Felser, and S. S. P. Parkin, Magnetic antiskyrmions above room temperature in tetragonal Heusler materials, *Nature (London)* **548**, 561 (2017).
- [32] Y. Tokunaga, X. Z. Yu, J. S. White, H. M. Rønnow, D. Morikawa, Y. Taguchi, and Y. Tokura, A new class of chiral materials hosting magnetic skyrmions beyond room temperature, *Nat. Comm.* **6**, 7638 (2015).
- [33] K. Karube, L. Peng, J. Masell, X. Yu, F. Kagawa, Y. Tokura, and Y. Taguchi, Room-temperature antiskyrmions and sawtooth surface textures in a non-centrosymmetric magnet with  $S_4$  symmetry, *Nat. Mater.* **20**, 335 (2021).